LUND UNIVERSITY

Light Scattering By Multiple Red Blood Cells

He, Jiangping; Karlsson, Anders; Swartling, Johannes; Andersson-Engels, Stefan

2003

[Link to publication](#)

Total number of authors:
4

Light Scattering By Multiple Red Blood Cells

Jiangping He, Anders Karlsson, Johannes Swartling,
and Stefan Andersson-Engels

Jiangping He

Department of Electroscience
Electromagnetic Theory
Lund Institute of Technology
P.O. Box 118
SE-221 00 Lund
Sweden

Center for Optical and Electromagnetic Research
Zhejiang university
P.R.China

Anders Karlsson

Department of Electroscience
Electromagnetic Theory
Lund Institute of Technology
P.O. Box 118
SE-221 00 Lund
Sweden

Johannes Swartling

Department of Physics
Lund Institute of Technology
P.O.Box 118
S-221 00 Lund
Sweden

Stefan Andersson-Engels

Department of Physics
Lund Institute of Technology
P.O.Box 118
S-221 00 Lund
Sweden

Abstract

The interaction of light with multiple red blood cells was systematically investigated by the finite-different time-domain method. The simulations show that the lateral multiple scattering between red blood cells is very weak. The polarization is shown to have an almost insignificant influence on the distribution of the scattered light. The numerical results were compared with three approximate methods: the superposition approximation, the Rytov approximation and the discrete dipole approximation. The agreement was very good.

1 Introduction

Blood analysis are useful diagnostic tools for many blood related diseases. A good understanding of the interaction of light with blood is a prerequisite for optical blood analysis. In this paper the scattering from multiple blood cells are numerically analyzed by a full wave method as well as by approximate methods.

It is known that the scattering and absorption of light in blood are largely governed by the red blood cells (RBCs). It is their refractive index, as well as their size, shape and orientation, that determine how light propagates. A previous paper [1], presents an investigation of the the interaction of light with one RBC. In particular the dependence of the scattered intensity on the wavelengths and the orientation of the RBC were analyzed. It was shown that approximate methods that utilize that the RBC is a weakly scattering object give accurate results. In experiments, the blood can be diluted so that the blood cells are sparsely distributed. In that case approximate multiple scattering methods based on the Monte-Carlo method are applicable [2]. The parameters used in these methods can be determined from a single blood cell calculation. In full blood, the concentration of RBC may be as high as 50%. Hence, the one RBC model may not be adequate.

In the case of high concentration of multiple RBCs the multiple scattering effects have to be considered. As the number of RBC in a system increases, the approximate methods that were successful for one RBC will eventually fail since they rely on that multiple scattering effects are small. The aim of this paper is twofold. One objective is to investigate the limitations of the finite difference time domain (FDTD) method and of the approximate methods. The other objective is to analyze the scattered intensities from one or multiple RBCs. That includes the analysis of cross polarization, the dependence on the orientation of the RBCs, and the dependence of the refractive index. The shapes of the RBCs are realistic (i.e. discocyte-like shape) in all of the calculations.

In the next section, Section 2, the geometry, material parameters, incident field and the scattered fields are defined. Section 3 contains descriptions of the FDTD method, the Rytov approximation, and the discrete dipole approximation (DDA) method. The numerical results are collected in Section 4 and in Section 5 some concluding remarks are given.
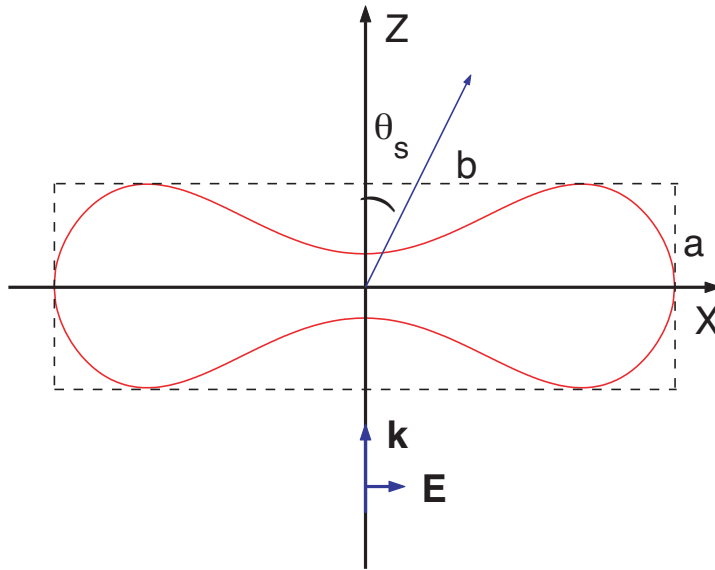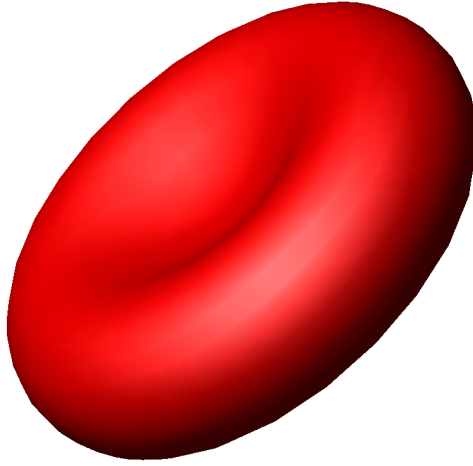
Figure 1: RBC cross section.

2 Preliminaries

The refractive index for the RBC is denoted n_1 and the refractive index of the surrounding blood plasma is denoted n_2. The absorption is neglected in both regions. The model of the disk-like normal RBC used in the simulations is defined in the references [3, 4] with a volume of the RBC of $94\,\mu\mathrm{m}^3$. The membrane of RBCs has a negligible influence on the scattered field, *cf.* [5, 6] and hence the RBC model does not include the membrane or any other internal structure. Figure 1 shows the cross section of the disk-like RBC model, where the enclosing box has height $a = 2.547\,\mu\mathrm{m}$ and length $b = 7.76\,\mu\mathrm{m}$. The three-dimensional (3D) shape is obtained by rotating the cross section around the $z-$axis. Figure 2 depicts the 3D picture of the disk-like RBC model. In the simulations, the incident wave is a time-harmonic linearly polarized plane wave. It propagates in the positive z-direction. The direction of the electric field is along the vector $\hat{\xi}$ which is a vector in the xy-plane. With the time convention $e^{-i\omega t}$, the complex incident electric field is given by

$$\boldsymbol{E}_{\mathrm{inc}}(z) = \hat{\xi} E_0 e^{ikz}, \tag{2.1}$$

where $k = n_2\omega/c_0$ is the wavenumber for the plasma and c_0 is the velocity of light in vacuum. In the numerical examples the RBCs are oriented so that their axis of symmetry is either parallel to the $z-$axis or to the $x-$axis, *cf.* figure 3. To interrelate the angular distributions of the scattered light of different incident angles, the scattering probability is calculated as a function of the zenith scattering angle θ_s (*cf.* figure 1) The scattering probability, $P(\theta_s)$, is defined as the integral of the

Figure 2: 3D RBC.

differential scattering cross section, $\sigma_{\mathrm{diff}}(\theta_s, \phi)$, over all azimuthal angles $\phi \in [0, 2\pi]$:

$$P(\theta_s) = \frac{\int_0^{2\pi} \sigma_{\mathrm{diff}}(\theta_s, \phi) \sin \theta_s d\phi}{\int_0^{2\pi} \int_0^{\pi} \sigma_{\mathrm{diff}}(\theta, \phi) \sin \theta d\theta d\phi}. \tag{2.2}$$

The differential cross section is defined by

$$\sigma_{\mathrm{diff}}(\theta, \phi) = r^2 \frac{< \boldsymbol{S}(r, \theta, \phi) \cdot \hat{r} >}{< \boldsymbol{S}_{\mathrm{inc}} \cdot \hat{z} >}, \tag{2.3}$$

where

$$< \boldsymbol{S}_s(r, \theta, \phi) > = \frac{1}{2} \mathrm{Re}\{\boldsymbol{E}(r, \theta, \phi) \times \boldsymbol{H}^*(r, \theta, \phi)\} \tag{2.4}$$

$$< \boldsymbol{S}_{\mathrm{inc}} > = \frac{1}{2} \mathrm{Re}\{\boldsymbol{E}_{\mathrm{inc}}(z) \times \boldsymbol{H}^*_{\mathrm{inc}}(z)\} = \frac{1}{2} \frac{n_2}{\eta_0} |E_0|^2 \hat{z} \tag{2.5}$$

are the time averages of the Poynting vector of the scattered and incident fields, respectively. Furthermore, $\hat{r}$ is the radial unit vector, $\boldsymbol{E}(r, \theta, \phi)$ is the scattered electric field, $\boldsymbol{H}^*(r, \theta, \phi)$ is the complex conjugate of the corresponding magnetic field, and $\eta_0 = 120\pi \ \Omega$ is the wave impedance of vacuum.

3 Methods

In this section the methods that are applied to the RBC problem are described briefly. The methods are the FDTD method and the three approximate methods: the superposition approximation, the Rytov approximation, and the DDA method.
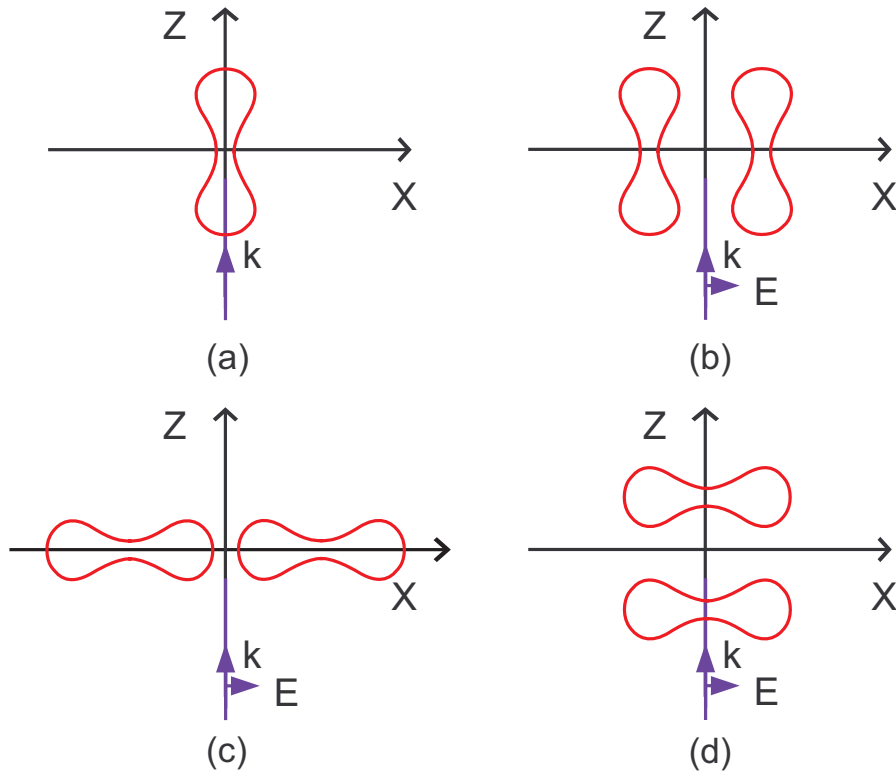
**Figure 3**: The different geometries used in the simulations.

3.1 FDTD: Yee's Method

The FDTD approach is general and flexible and was recently applied to biological scattering problems: [7–10]. It enables the simulation of scattering from inhomogeneous objects of arbitrary shape. Today it is one of the best full wave methods for accurate simulations of the scattering of light from a small number of blood cells. Readers interested in FDTD are recommended the book by Taflove [7], which gives a good overview. The FDTD algorithm numerically solves the Maxwell's curl equations in time domain. In order to get the angular far-field distribution of the scattered light, several techniques are required:

Absorbing boundary condition Because of the finite computational domain, the values of the fields on the boundaries must be defined so that the solution region appears to extend infinitely in all directions. With no truncation conditions, the scattered waves will be artificially reflected at the boundaries leading to inaccurate results. The perfectly matched layer (PML) ABC suggested by Berenger [11] has been implemented in the three-dimensional FDTD program and is used in the examples in this paper.

Total field/scattered field Since this work considers the scattering patterns, the total field/scattered field formulation is used. The computational grid is divided
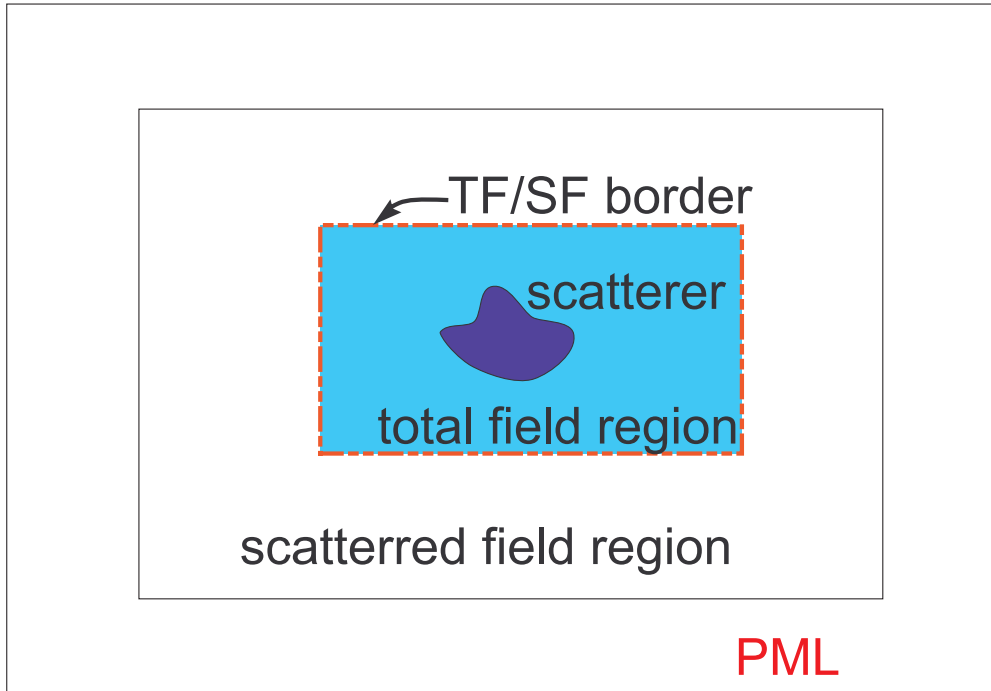
Figure 4: The regions used by FDTD.

into two regions. The total field region encloses the scatterers whereas the scattered field region, where only the scattered field components are stored, encloses the total field region, as illustrated in Figure 4. At the border between the two regions, special connecting conditions are required, where the incident field is either added or subtracted from the total field. The details of the connecting region can be found in [7].

Far-Field Transformation The FDTD is inherently a near-field method. To determine the far-field scattering pattern, the near-field data is transformed to the far-field by the near-field to far-field (NFFF) transformation. The details of the NFFF technique can be found in [7].

3.2 The Discrete Dipole Approximation

The Discrete Dipole Approximation (DDA) is closely related to the method of moments [12]. The principle of the method is as follows: The scattering volume is divided into N parts. Each part is small enough to be represented by a dipole moment. Linearity of the medium implies that the induced dipole moment is equal to the electric field in the volume multiplied by the polarizability of the volume. The electric field is a superposition of the field from the sources external to the object and the electric field from the sources inside the object, in this case the induced dipoles. The field from the external sources is the incident plane wave and hence
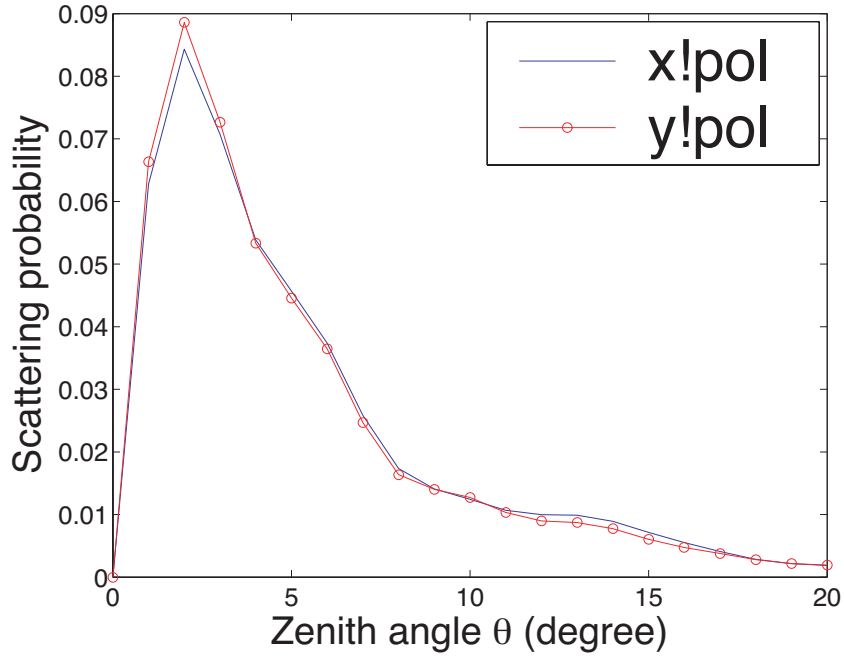
Figure 5: The scattering probabilities of the RBC in figure 3(a) for polarization along the $\hat{x}-$ and the $\hat{y}-$directions.

the electric field in volume j is given by

$$\boldsymbol{E}(\boldsymbol{r}_j) = \boldsymbol{E}_{\mathrm{inc}}(\boldsymbol{r}_j) + \sum_{k \neq j} \mathbf{A}(\boldsymbol{r}_j, \boldsymbol{r}_k) \cdot \boldsymbol{p}(\boldsymbol{r}_k) \qquad (3.1)$$

The term $\mathbf{A}(\boldsymbol{r}_j, \boldsymbol{r}_k) \cdot \boldsymbol{p}(\boldsymbol{r}_k)$, where $\mathbf{A}(\boldsymbol{r}_j, \boldsymbol{r}_k)$ is the Green dyadic, is the electric field at a position $\boldsymbol{r}_j$ from a dipole at position $\boldsymbol{r}_k$ and can be found in basic textbooks in electromagnetic theory. The equation is usually not solved by direct inversion. Instead the conjugate gradient method is applied. A more detailed description of the DDA method is given in [12, 13].

3.3 Superposition

The superposition approximation is based on the assumption that multiple scattering effects are small between the cells. Each RBC is viewed as a scattering object and the multiple scattering effects between the RBCs are neglected. The advantage is a reduction of the CPU-time and the required RAM of the computer. The far-field pattern is calculated by the FDTD method for each RBC, and then the far-fields are added. In our RBCs simulation models, the scattering objects are identical and have the same orientation. The far-fields of the RBCs are the same, except for the phase shift. Thus, it is enough to perform a simulation for one RBC and add a phase shift to get the total far-field of the RBCs. Given the far-field $\boldsymbol{E}(\theta, \phi, r)$ of one RBC with the origin located at the center of the RBC, the far field expression
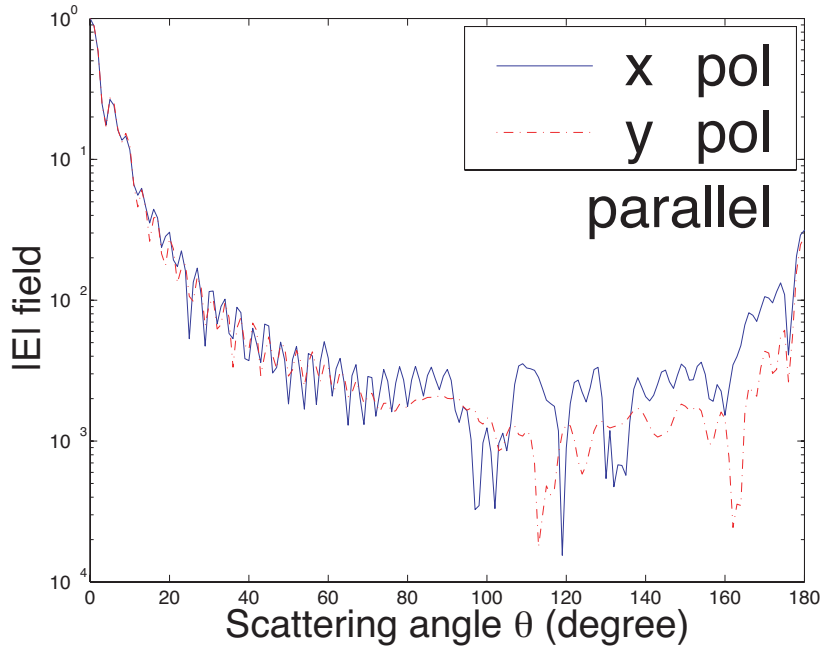
Figure 6: The absolute value of the far-field amplitude of the electric field for the RBC in figure 3 (a). The solid curve shows the far-field in the $xz-$plane for the incident field polarized in the $x-$direction and the dashed curve is the far-field in the $yz-$plane for an incident field polarized in the $y-$direction.

for the configurations of N RBCs equation (3) reads:

$$\boldsymbol{E}_{2RBC}(\theta, \phi) = \boldsymbol{E}(\theta, \phi)(\sum_{n=1}^{N} e^{ik\hat{r}\cdot\boldsymbol{d}_n}) \tag{3.2}$$

where $\hat{r} = (\sin\theta\cos\phi, \sin\theta\sin\phi, \cos\theta)$, $\boldsymbol{d}_n$ is the translated vector of RBC number n relative to the origin and where k is the wave number for the plasma. The method gives accurate results as long as the blood cells are located in directions lateral to the $z-$axis.

3.4   The Rytov approximation

The Rytov approximation is a frequently used method in tomography, [14, 15]. It is then utilized for the inverse scattering problem of determining the permittivity or conductivity of an object. In this paper it is applied in its simplest form to the scattering of a plane wave from objects in a homogeneous lossless medium. The reason the simplest form is used is somewhat based on the reference [16] where it is claimed that the back-scattered amplitude is very small compared to the forward-scattered amplitude. The method can be explained as follows: Consider an object that occupies the volume V. Let the index of refraction be n_1 for the object and n_2 for the surrounding medium. The incident wave is given by Eq. (2.1). The

Figure 7: The absolute value of the far-field amplitude of the electric field for the RBC in figure 3 (a). The solid curve shows the far-field in the $yz-$plane for the incident field polarized in the $x-$direction and the dashed curve is the far-field in the $xz-$plane for an incident field polarized in the $y-$direction.
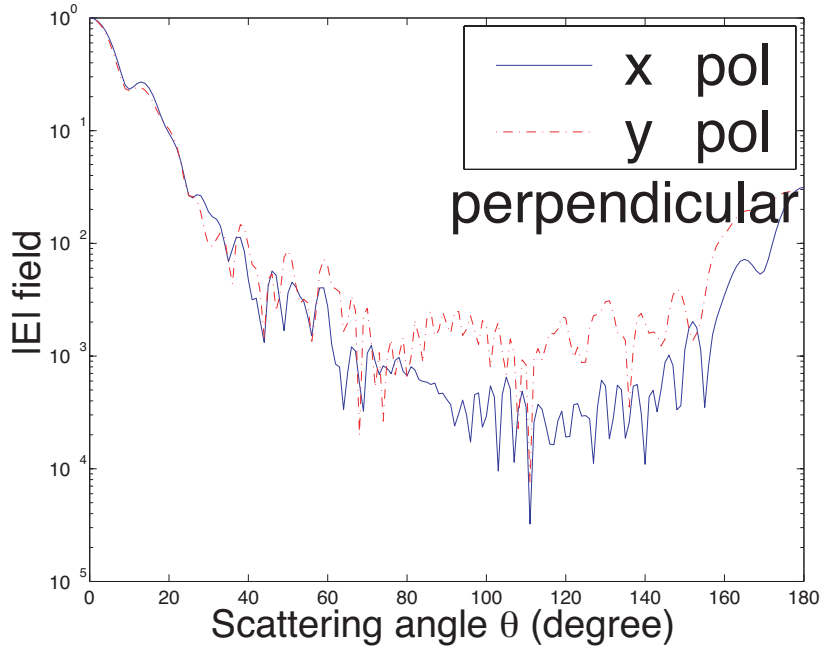
approximation assumes that when the wave passes the object, the phase of the wave is shifted while its amplitude and polarization are unaltered. The wave is assumed to travel along straight rays parallel to the z-axis, *i.e.*, along lines $\boldsymbol{r} = (x, y)$. Let $d(x, y)$ be the total distance the ray travels inside the scattering object. If $z = z_1$ is a plane behind the object, the total electric field in that plane reads

$$\boldsymbol{E}(x, y, z_1) = \hat{x} E_0 e^{ik_0(n_2 z_1 + (n_1 - n_2)d(x,y))} \tag{3.3}$$

where $k_0 = \omega/c_0$ is the wave number in vacuum. Thus the phase is shifted an angle $k_0(n_1 - n_2)d(x, y)$ compared to the incident wave. The far-field amplitude is given by the near-field to far-field transformation, *cf.* [7], *i.e.*,

$$\boldsymbol{F}(\theta, \phi) = i \frac{k^2}{4\pi} E_0 e^{ikz_1} \hat{r} \times \iint\limits_{S} (\hat{y} - \hat{r} \times \hat{x}) \left(e^{ik_0(n_1 - n_2)d(x,y)} - 1 \right) e^{-ik\hat{r}\cdot\boldsymbol{r}} \mathrm{d}x\mathrm{d}y \tag{3.4}$$

where S is the plane $z = z_1$. Notice that the integrand is zero outside the projection of the blood cells on the plane $z = z_1$. All reflections of the wave are neglected. Consequently, the approximation gives a far-field amplitude that is only accurate for angles $\theta < \pi/2$. Despite these approximations the calculated far-field pattern is quite accurate for the one RBC case []. The advantage of the Rytov approximation is that it is simple and can easily be implemented on a computer.
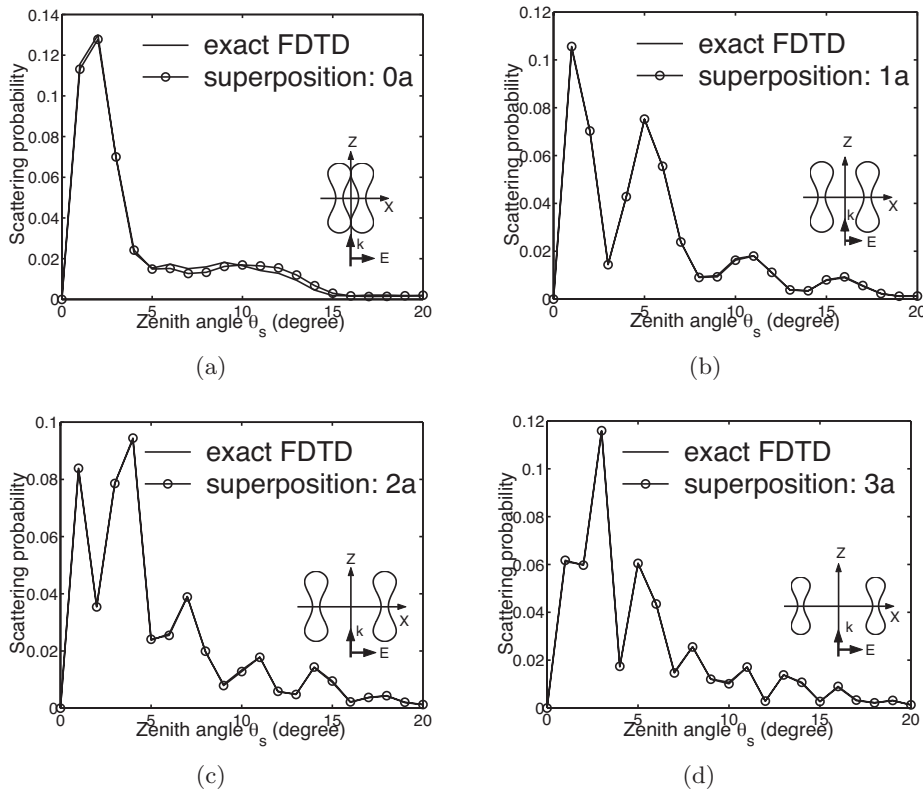
Figure 8: Scattering probability for the geometry in figure 3 (b) with 4 different separation distances. Figures (a)-(d) are the results with separation distances equal to $0a$, $1a$, $2a$ and $3a$, respectively, where a is the thickness of the RBC cross section, *cf.* figure 1.

4 Results and discussions

In this section the scattering properties of the RBCs are investigated by the FDTD method, the superposition approximation, the Rytov approximation and the DDA method. The simulation program $SEMCAD$ [17] was used for the FDTD simulations of the far-field scattering pattern. In all the FDTD simulation cases, the grid space was adaptively set between $\lambda/10$ and $\lambda/20$, in order to yield accurate results. The simulations in this paper indicate that the Rytov approximation is somewhat faster than the DDA method. Both of them are considerably much faster than the FDTD method. The Rytov approximation method is the most memory efficient method of the three. In the numerical examples, the index of refraction of the RBC and the plasma is $n_1 = 1.406$ and $n_2 = 1.345$, respectively, except in section 4.4 where the influence of the index of refractive is investigated.

4.1 The influence of the polarization

First, the cross-polarization effect is analyzed. It is anticipated that cross polarization can appear in flowing blood since the RBCs tend to align in a direction
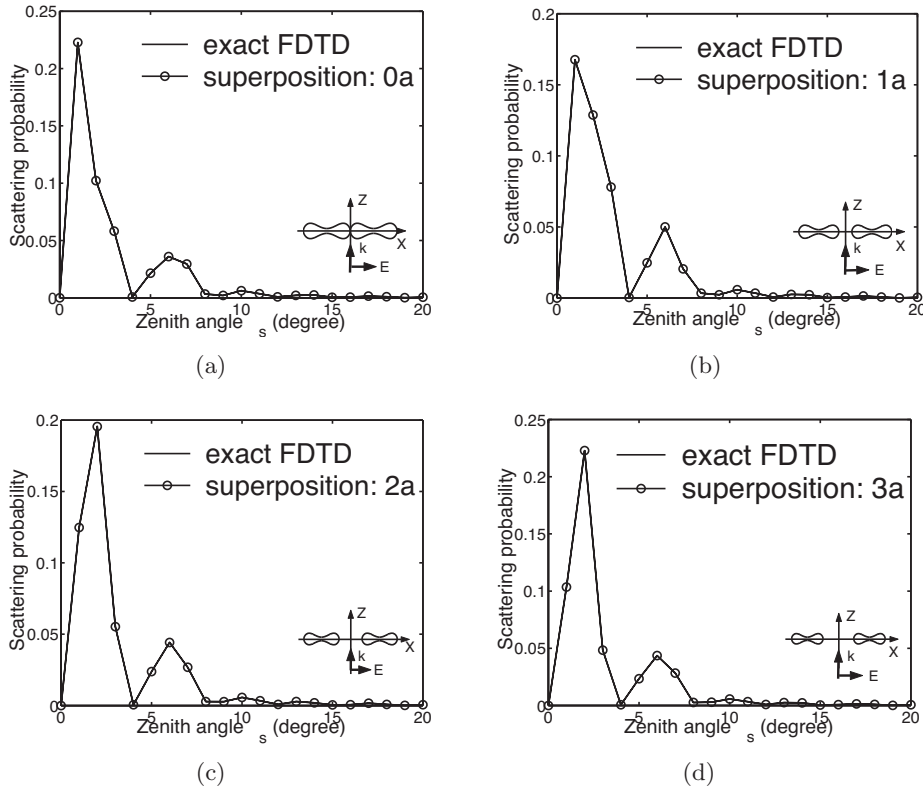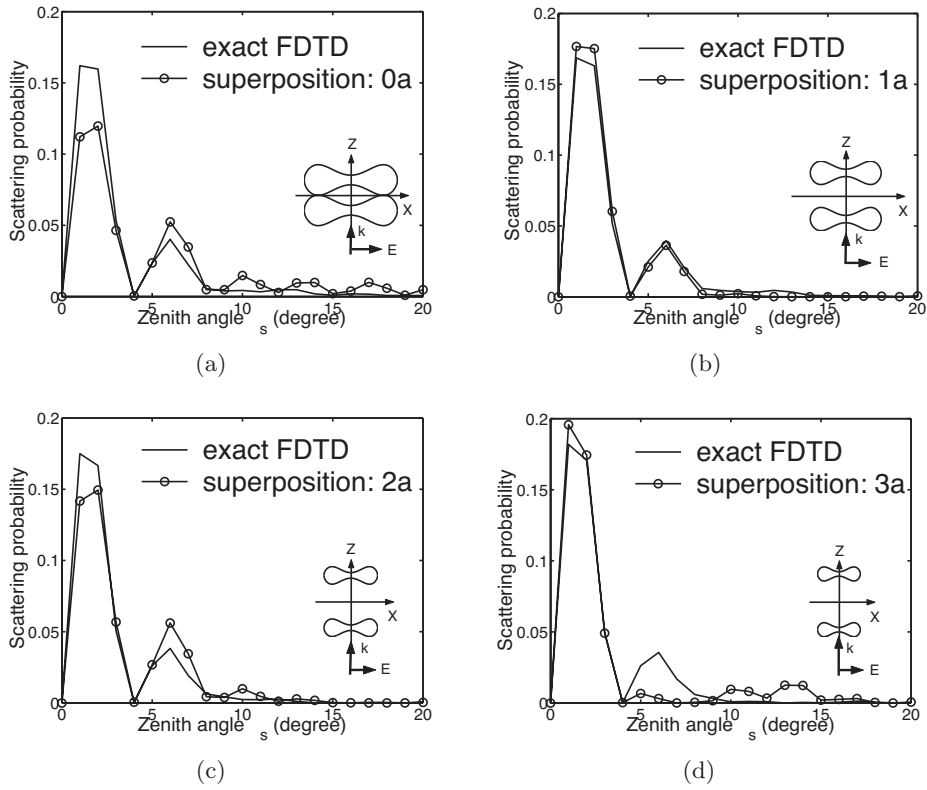
Figure 9: The same case as in figure 8 but for model (c).

perpendicular to the flow direction. The question is if the effect is strong enough to be measurable. The far fields were calculated using the model presented in figure 3(a), for two orthogonal polarizations, one with $\hat{\xi} = \hat{x}$, *i.e.*, with the electric field in the $\hat{x}$-direction, and the the other with $\hat{\xi} = \hat{y}$, cf Eq. (2.1). The scattering probability patterns are shown in figure 5. Since the scattering probability, *cf.* Eq. (2.2), is an averaged value over the azimuthal angle ϕ, the polarization effect almost disappears. This conclusion is in agreement with T-matrix results [18]. Figure 6 shows the absolute value of the electric far-field amplitude in the $xz-$plane nd the $yz-$plane in the cases of polarization in the $\hat{x}-$ and the $\hat{y}-$direction, respectively. The corresponding graphs for cross polarization are shown in figure 7. As seen from the graphs the far-field is polarization dependence is very weak, in particular in the forward direction. There will be a small cross-polarization if all RBCs are aligned as in figure 3(a). Very accurate measurements are required in order to detect the cross polarization.

4.2 The scattering probability for model (b)-(d)

To investigate the dependence of the distance between two RBCs, systematic simulations were conducted by accurate FDTD calculations, as well as by superposition and by the Rytov approximation. Three cases were simulated. For each case, the

**Figure 10**: The same case as in figure 8 but for model (d).

scattering probabilities were calculated for different distances between two RBCs (*i.e.*, 0*a*, 1*a*, 2*a* and 3*a*, where *a* is the thickness of the RBC, *cf.* Figure 1).

4.2.1 Model (b) case

Figure 8 shows the influence the distance between cells has on the scattering probability. The scattering pattern becomes more complex when the RBCs distance increases. The superposition method is accurate, even when the two RBCs touch. These results emphasize that the lateral multiple-scattering is very weak between RBCs.

4.2.2 Model (c) case

The same simulations as in the previous case were conducted for the geometry in figure 3(c). The results are presented in figure 9. The scattering patterns are almost independent of the lateral distance. The superposition method is accurate due to the weak lateral multiple-scattering between RBCs. Also the Rytov approximation provides very similar results (not shown).
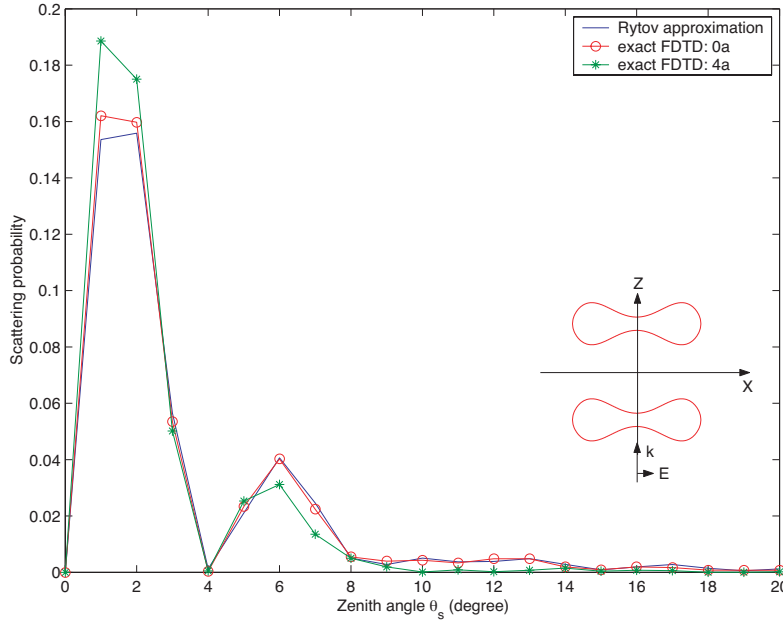
Figure 11: The scattering probability obtained by the FDTD and the Rytov approximation of for the geometry in figure 3(d) with the distances $0a$ and $4a$ between the RBCs, respectively.

4.2.3 Model (d) case

The scattering patterns for the geometry in figure 3(d) are similar to that of model (c), see figure 10. The superposition method does not work as well as in models (b) and (c). This means that the multiple-scattering along the incident wave direction is more pronounced than in the lateral case and cannot be neglected. The Rytov approximation results of model (d) also support this conclusion, see figure 11. Since the simplest form of the Rytov approximation is used, there is no difference between the simulation result using different distances in model (d), cf Eq. (3.3). The DDA method was also applied to the model (d). Figure 12 shows the result when the RBCs distance equals $0a$ for model (d). It is seen that the DDA method can deal with the multiple-scattering.

4.3 The scattering probability for multiple RBCs

As mentioned in section 3.3, the superposition method provides accurate results as long as the blood cells are located in directions lateral to the incident wave. Figure 13 shows the scattering patterns of multiple RBCs. The simulation geometry is the same as in figure 3(b) except that the number of RBCs is changed. Our simulation results show that one may calculate the scattering probability for many parallel RBCs by dividing the large simulation domain into small and computable subdomains along directions perpendicular to the incident wave direction and using the superposition method.
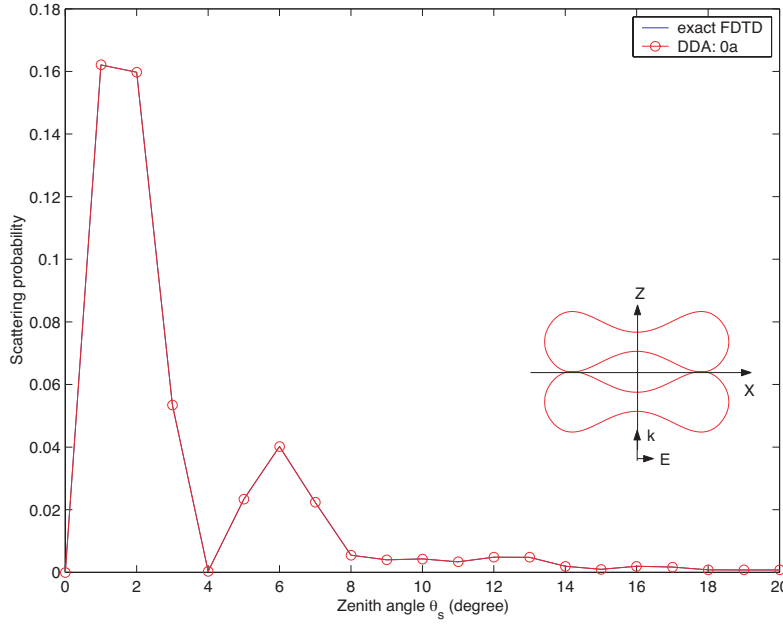
Figure 12: The scattering probability obtained from the FDTD and the DDA simulations for the geometry on figure 3(d) with the distance $0a$ between the RBCs.

4.4 The dependence of refractive index

In order to investigate the dependence of the refractive index, the refractive index of the plasma, n_2, was altered, while the refractive index of the RBC was fixed at $n_1 = 1.406$. Three different index of refraction were used in this case (*i.e.*, $n_2 = n_1/1.020, n_1/1.010, n_1/1.007$). It is interesting that the normalized scattering patterns of these three cases are almost the same. Since the relative refractive index is very low, the scattering can be described by the Born approximation [19]. According to the Born approximation, the scattered field of the RBC reads,
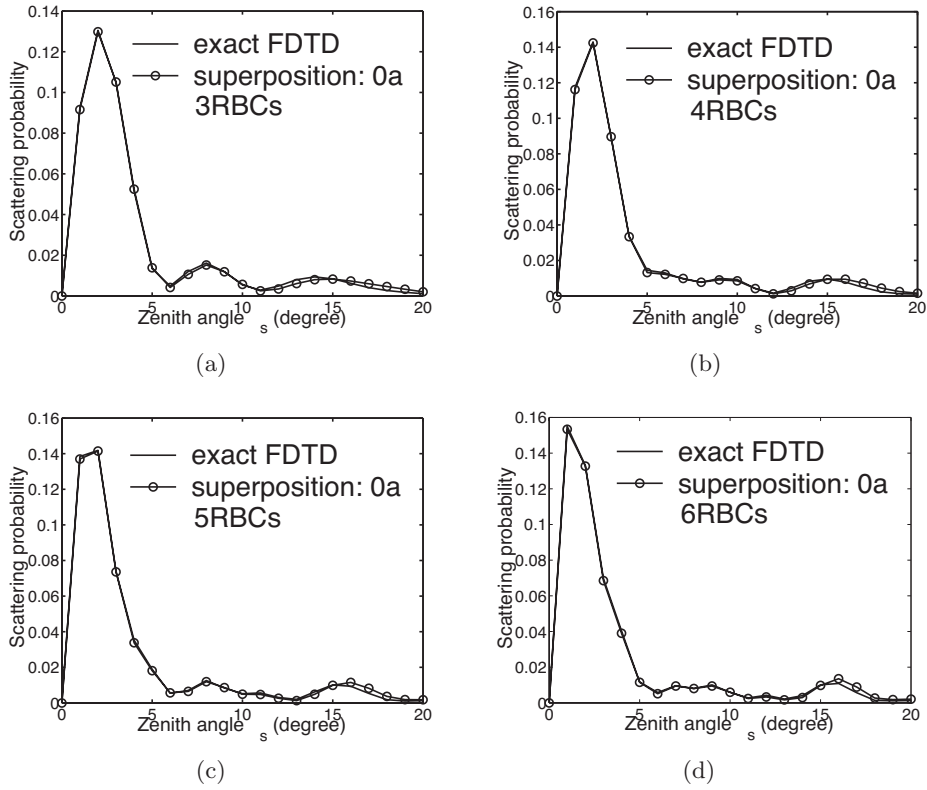
$$\boldsymbol{E}_s = -\frac{k^2 e^{ikr}}{4\pi r}\hat{k}_s \times (\hat{k}_s \times \hat{e}_i)(n_{ref}^2 - 1)\iiint\limits_{RBC} dV e^{i(\boldsymbol{k}_i - \boldsymbol{k}_s)\cdot\boldsymbol{r}'}, \qquad (4.1)$$

where $n_{ref} = n_1/n_2$. The ratio of the scattered far fields with different background reads,

$$\frac{\boldsymbol{E}'}{\boldsymbol{E}} \sim \left(\frac{k'}{k}\right)^2 \frac{n_{ref}'^2 - 1}{n_{ref}^2 - 1}[1 + O(\delta k)] \qquad (4.2)$$

where k and k' are the wave number in the background and $\delta k = k' - k$. Thus the ratio of the radiated powers reads,

$$\frac{P'}{P} \sim \left[\frac{n_{ref}'^{-2} - 1}{n_{ref}^{-2} - 1}\right]^2 \qquad (4.3)$$

Figure 13: The same case as in figure 8 but with more than two number of RBCs are given in the label of the corresponding figures.

Table 1: The radiation powers of RBC with different background refractive index.

n_{ref}	1.045	1.020	1.010
P (FDTD)	1.39×10^{-13}	3.33×10^{-14}	8.72×10^{-15}
P (equation 4.3)	1.60×10^{-13}	3.40×10^{-14}	8.76×10^{-15}

In table 1, the radiated powers with different background refractive index are listed. The results using equation 4.3 with $n'_{ref} = 1.007$, $P' = 4.33 \times 10^{-15}$ are also given in the table. The FDTD simulation results and that of Born approximation have the same order of magnitude. The accuracy of the Born approximation improves as the relative refractive index approaches one.

5   Conclusions

The scattering from several RBCs are analyzed. From the simulation results, it is seen that there is a weak polarization dependence in the far-field pattern from one RBC. This is agreement with the published results by T-matrix calculations [18]. It implies that there are cross-polarization effects when polarized light propagates through a sample of blood if the blood cells are aligned. The effect is weak, in

particular in the forward direction and it might not be possible to detect the cross polarization in an experiment. The scattering probability patterns are not sensitive to the polarization due to the integration in the azimuthal angle. The general and flexible numerical approach FDTD was employed to study the multiple-scattering properties between RBCs. The calculations show that the lateral multiple-scattering between RBCs is very weak. As a result of this, approximate methods are accurate. Meanwhile, the multiple-scattering between RBCs located along the incident wave direction cannot be neglected. Hence, superposition and the simplest form of Rytov approximation do not give accurate results in that case. However, the results of the DDA method, which is a more accurate method, agrees with the FDTD results.

For the applications in this paper, the DDA method is faster than FDTD and requires less memory. Hence, it is a very strong alternative to FDTD. The Rytov approximation is less accurate than DDA and FDTD methods. However, it is a very simple method that can easily be implemented on a computer. It also give accurate results for the geometry in figure 3(c).

References

[1] Jiangping He, A. Karlsson, J. Swartling, S. Andersson-Engels. Numerical simulations of light scattering by red blood cells *Technical report LUTEDX/(TEAT-7116)*, Lund Institute of Technology, Department of Electroscience, P.O. Box 118,S-221 00 Lund, Sweden, 2003.

[2] L. Wang, S. L. Jacques, L. Zheng. MCML – Monte Carlo modeling of light transport in multi-layered tissues *Computer Methods and Programs in Biomedicine*, 47:131–46, 1995.

[3] E. Evans and Y. Fung. Improved measurement of the erythrocyte geometry. *Microvascular research*, 4:335–347, 1972.

[4] Peter Alsholm. Light scattering by individual and groups of spheroidal particles. Technical Report LRAP-200, Lund report on atomic physics, Lund Institute of Technology, August 1996.

[5] R. A. Meyer. Light scattering from red blood cell ghosts: sensitivity of angular dependent structure to membrane thickness and refractive index. *Appl. Opt.*, 16:2036–2037, 1977.

[6] J. C. Lin and A. W. Guy. A note on the optical scattering characteristics of whole blood. *IEEE Trans. Biomed. Eng.*, 21:43–45, 1974.

[7] Allen Taflove. *Computational Electrodynamics: The Finite Different Time Domain Method.* Artech, Boston, 1995.

[8] R. Drezek, A. Dunn and R. Richard-Kortum. Light scattering from cells: finite-different time-domain simulations and goniometric measurements. *Applied Optics*, 38(16):3651–3661, June 1999.

[9] R. Drezek, M. Guillaud, T. Collier, A. Malpica, C. Macaulay M. Follen and R. Richards-Kortum. Light scattering from cervical cells throughout neoplastic progression: influence of nuclear morphology, DNA content, and chromatin texture. *Journal of Biomedical optics*, 8(1):7–16, January 2003.

[10] R. Drezek, A. Dunn and R. Richards-Kortum. A pulse finite-difference time-domain (fdtd) method for calculating light scattering from biological cells over broad wavelength ranges. *Optics Express*, 6(7):147–157, March 2000.

[11] J. P. Berenger. A perfectly matched layer for the absorption of electromagnetic waves. *J. Computational Physics*, 114:185–200, 1994.

[12] B. T. Drain and Flatau. Discrete-dipole approximation for scattering calculations. *J. Opt. Soc. Am. A*, 11:1491–1499, 1994.

[13] B. T. Draine. *Light Scattering by Nonspherical Particles: Theory, Measurements, and Applications*. Academic Press, New York, 2000.

[14] V. I. Tatarski. *Wave propagation in a turbulent medium*. McGraw-Hill, New York, 1961.

[15] Avinash C. Kak and Malcolm Slaney. *Principles of computerized tomographic imaging*. IEEE Press, New York, 1988.

[16] Victor Twersky. Interface effects in multiple scattering by large, low-refracting, absorbing particles. *Journal of the Optical Society of America*, 60(7):908–914, July 1970.

[17] http://www.semcad.com/

[18] A. M. K. Nilsson, P. Alsholm, A. Karlsson and S. Andersson-Engels. T-matrix computations of light scattering by red blood cells. *Applied Optics*, 37(13):2735–2748, May 1998.

[19] Leung Tsang, Jin Au Kong and Kung-Hau Ding. *Scattering of Electromagnetic Waves: Theories and Applications*. John Wiley and Sons. Inc, New York, 2000.